metals

MDPI

Article

Effects of Sinter-HIP Temperature on Microstructure and Properties of WC–12Co Produced Using Binder Jetting

Ivan Goncharov [1,*], Marco Mariani [1], Gian Pietro De Gaudenzi [2], Anatoliy Popovich [3], Nora Lecis [1] and Maurizio Vedani [1]

[1] Department of Mechanical Engineering, Politecnico di Milano, 20156 Milan, Italy
[2] HI.Lab, F.I.L.M.S. S.p.A., OMCD Group, 28877 Anzola d'Ossola, Italy
[3] Institute of Machinery, Materials and Transport, Peter the Great St. Petersburg Polytechnic University, 195251 St. Petersburg, Russia
* Correspondence: ivan.goncharov@polimi.it

Abstract: This study investigates the influence of different sinter-HIP temperatures and binder saturation levels on the microstructure and properties of WC–12Co cemented carbide, produced using binder jetting. The sinter-HIP process was performed at 1400 °C, 1460 °C, and 1500 °C and binder saturation levels of 60% and 75% were selected during printing. The binder saturation proved to affect the repeatability of the manufacturing process and the sturdiness of the green models. The increase of the sintering temperature from 1400 °C to 1460 °C is correlated with an increase in the density. Nonetheless, a further raise in temperature to 1500 °C leads to significant grain coarsening without clear advantages in terms of porosity reduction. Both the transverse rupture strength and Vickers hardness increase when the sinter-HIP temperature rises from 1400 °C to 1460 °C, where the typical results for traditionally manufactured WC–12Co are met, with a comparable grain size. The transverse rupture strength and Vickers hardness then decrease for samples treated at 1500 °C. Finally, potential issues in the manufacturing process are identified and correlated with the defects in the final components.

Keywords: cemented carbides; binder jetting; additive manufacturing; sinter-HIP; WC-Co; microstructure

Citation: Goncharov, I.; Mariani, M.; De Gaudenzi, G.P.; Popovich, A.; Lecis, N.; Vedani, M. Effects of Sinter-HIP Temperature on Microstructure and Properties of WC–12Co Produced Using Binder Jetting. *Metals* **2024**, *14*, 132. https://doi.org/10.3390/met14010132

Academic Editors: Johannes Pötschke, Shuigen Huang and Inigo Agote

Received: 4 December 2023
Revised: 12 January 2024
Accepted: 18 January 2024
Published: 22 January 2024

1. Introduction

Cemented carbides represent a class of composite materials featuring hard carbides embedded in a ductile metallic binder phase, offering a favorable combination of high hardness, toughness, and wear resistance. The ternary system W–Co–C and the pseudobinary WC–Co have been extensively studied due to their outstanding mechanical properties and cutting performance, making them widely used in various industrial applications. The main factors that influence their mechanical properties are the content of the binder phase and the size and the distribution of carbide grains [1–3]. Notably, it has been established that the enhancement of wear resistance exhibits a linear correlation with the reduction in the square root of the WC grain size, regardless of the cobalt content [4]. Sintering these WC/Co composites at temperatures between 1380 °C and 1450 °C ensures high density (>99% of the theoretical density) and minimal residual porosity, a feat facilitated by the proper miscibility of W and C in cobalt and the favorable wetting properties of the liquid/solid interface during sintering. Moreover, sintering at these temperatures yields not only the desired high microhardness but also a highly uniform microstructure of the material [3].

Additive manufacturing (AM) is a group of manufacturing technologies that are used to produce parts by shaping materials, usually in a layer-by-layer manner, through the section of computer-aided design (CAD) models. This approach holds considerable advantages and presents extensive potential for fabricating geometrically intricate

cemented carbide components, a feat often unattainable through traditional powder metallurgy methods.

In recent years, several studies have been conducted on the use of additive manufacturing (AM) techniques for cemented carbides. Most of the research refers to the two main groups of AM techniques. The first group consists of hot-forming techniques, which assumes the forming of a dense component during the printing process. This group includes laser and electron beam powder bed fusion (LPBF and EPBF) [5–9] and directed energy deposition (DED) techniques [10,11]. In the case of cemented carbides, the latter is mainly used for coatings rather than to form a three-dimensional shape part. The second group includes multiple-step processes, in which forming and densification are performed at separate stages with different equipment. Namely, the most relevant are as follows: fused deposition modelling (FDM) [12,13], selective laser sintering (SLS) [14], in which the fusion occurs only in the polymer shells of the powders, and binder jetting additive manufacturing (BJAM) [15–18]. Multi-step processes combine the forming of a green-body with a subsequent thermal treatment (debinding–sintering) as in traditional powder metallurgy. Among all others, the BJAM technique appears to be the most promising technique to produce near-net-shape WC-based parts, because the printing process of the green bodies with the organic binder occurs at a low temperature, the resolution of the process is high, and densification using sintering or sinter-HIPing is performed separately, following principles and recommendations similar to those of traditional and well-developed manufacturing technologies [19,20]. Recent studies on binder jetting revealed the formation of coarse-grained cemented carbides after sintering [21] at temperatures higher than 1400 °C, and superior wear resistance in comparison with similar conventionally produced cemented carbides, with a substantial leap in the geometrical complexity of potential parts [22].

In previous works, we investigated the influence of the powder on the microstructure, the phase composition, and the properties of WC–Co using binder jetting and pressureless and pressure-assisted sintering [23], and the influence of printing parameters [24] on the density of the sintered samples. The current study is dedicated to identifying the effects of different sintering conditions on the densification and grain growth mechanisms within the microstructure of dense components, in combination with the binder saturation level adopted during the printing process. This is known to affect the particles packing in the powder bed, the accuracy of the green parts, and possibly the final carbon content. Additionally, defects and inaccuracies are analyzed to define recommendations and guidelines for future studies.

2. Materials and Methods

For this study, the AM WC702 powder was used with a nominal composition of WC–12Co (wt.%), which is one of the typical industrial cemented carbide compositions, provided by Global Tungsten & Powders Corp. (Towanda, PA, USA). The organic binder used in the work is the ExOne Inc (part of Desktop Metal Company, Burlington, MA, USA) proprietary water-based diethylene glycol monoethyl ether ($C_6H_{14}O_3$) product (code: BA-005), that forms polyethylene glycol (PEG) upon curing.

The powder surface and sections of powder particles were visually analyzed via ZEISS SIGMA 500 scanning electron microscopy (Carl Zeiss AG, Jena, Germany). For each sample, 5 images with at least 200 measurements of grains were performed to determine the average size and distribution of the grains [25].

The phase composition was analyzed using an X-ray diffractometer Rigaku Smartlab 2 (Rigaku Corporation, Tokyo, Japan). The measurement was performed with a Cu-Kα radiation (λ = 1.5406 Å) at a scanning rate of 1° min^{-1}, from 10° to 100° and with a step size of 0.02°.

Parallelepiped-shaped samples (6 × 6 × 60 mm^3) were printed horizontally alongside with printhead direction, using an ExOne Innovent+ machine. The printing was performed with 2 sets of parameters; the most relevant are summarized in Table 1. The selected values

of binder saturation (namely 60% and 75%) proved to be associated with the optimal results reported in previous works [23,24].

Table 1. Binder jetting printing parameters.

Sample	50/60	50/75
Layer thickness	50 µm	50 µm
Binder saturation	60%	75%
Drying time	12 s	12 s
Recoat speed	10 mm/s	10 mm/s

After printing, the samples were cured at 180 °C for 6 h in air to polymerize the organic binder. Green models of the samples were then debinded at 500 °C for 4 h in nitrogen. Densification was performed at different conditions: 1400 °C, 1460 °C, and 1500 °C for 3 h under a vacuum, with subsequent sinter-HIP processing under a 35 bar Ar pressure for 20 min at 1400 °C, 1460 °C, and 1500 °C.

The microstructure of the transverse sections of the samples (along a plane parallel to building direction) was analyzed using SEM ZEISS SIGMA (Carl Zeiss AG, Jena, Germany) 500 with the following parameters: acceleration voltage 20 kV, working distance 6.8–8.8 mm. The density was measured using the Archimedes method in accordance with [26]. Specimens were mechanically characterized using Vickers hardness (HV) measurements with an applied load of 100 kgf for 15 s on the polished surfaces [27] and using 3-point bending tests on the ground and chamfered type B samples with a constant load displacement rate of 0.5 mm min^{-1} [28]; the span between the support rods was set at 14.5 mm to assess the transverse rupture strength (TRS), with 3 specimens for each condition.

3. Results

3.1. Powder Characterization

The polished sections of the particles (Figure 1) show a highly spherical aspect and a microstructure consisting of fine WC within homogeneously distributed Co. In contrast with powders from previous works [24], no coarse WC grains were observed, and a weak diffraction peak of secondary W_2C was noticed in the XRD analysis (Figure 2). Both phases are uniformly distributed; however, some particles exhibit relevant inner porosity, likely due to the incomplete densification of the granules during their spheroidization process.

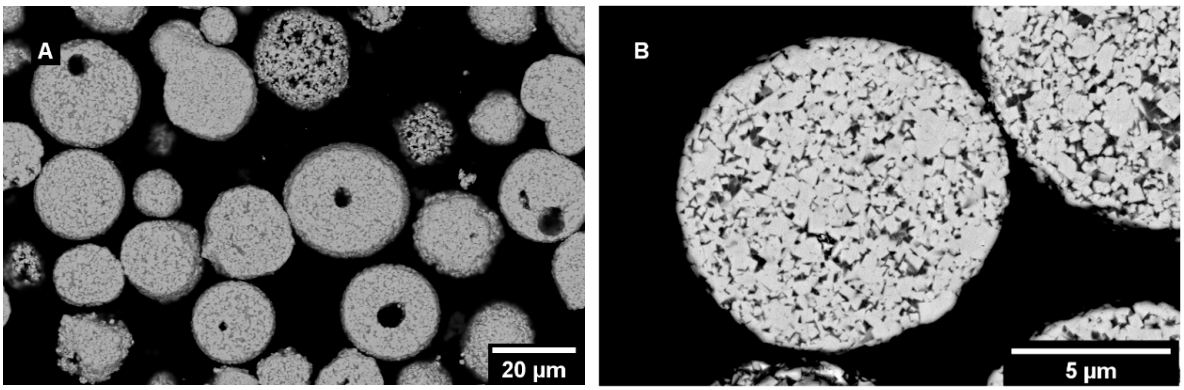

Figure 1. SEM images of the polished sections of WC–12Co powder, (**A**) general view; (**B**) single particle.

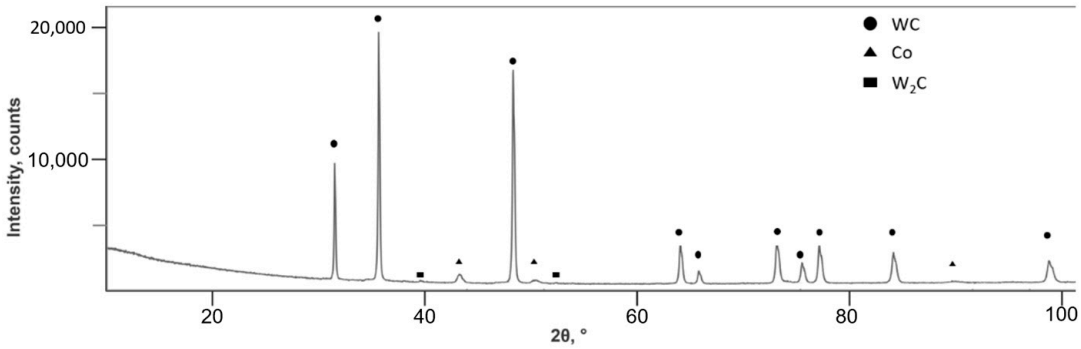

Figure 2. XRD of the WC–12Co powder.

3.2. Microstructural Characterization

The microstructure of the transverse section of the 50/60 samples after sinter-HIP processing is shown in Figure 3. At a lower magnification, the samples sintered at 1400 °C (Figure 3A) display some randomly located equiaxial-shaped pores. At a higher magnification (Figure 3B), the microstructure presents uniformly distributed fine grains of WC with an average size of about 1.65 µm, and some coalesced coarse grains with a dimension up to 15 µm. To understand this bi-modal nature of the WC grains, the size of the grains was evaluated, and the results were divided into coarse grains, which are above 5 µm, and fine grains. The total area occupied by the coarse grains (>5 µm) is about 11%, as summarized in Table 2. Cobalt is distributed uniformly in between the WC grains. Nonetheless, it can be noticed that cobalt tends to accumulate within the voids between the coarse grains, forming large pools, as shown in the higher magnification micrographs (Figure 3C).

Elevating the sinter-HIP processing temperature to 1460 °C results in a significant reduction in residual porosity, and the final relative density is raised above 99% (see Table 2). Simultaneously, there is an enlargement in the volume occupied by the coarse grains (visible in Figure 3D,F) to approximately 15%. Despite this temperature increase, there is no significant growth observed in the average size of the tungsten carbide grains, which remains at 1.60 µm, as outlined in Table 2 and depicted in Figure 3E.

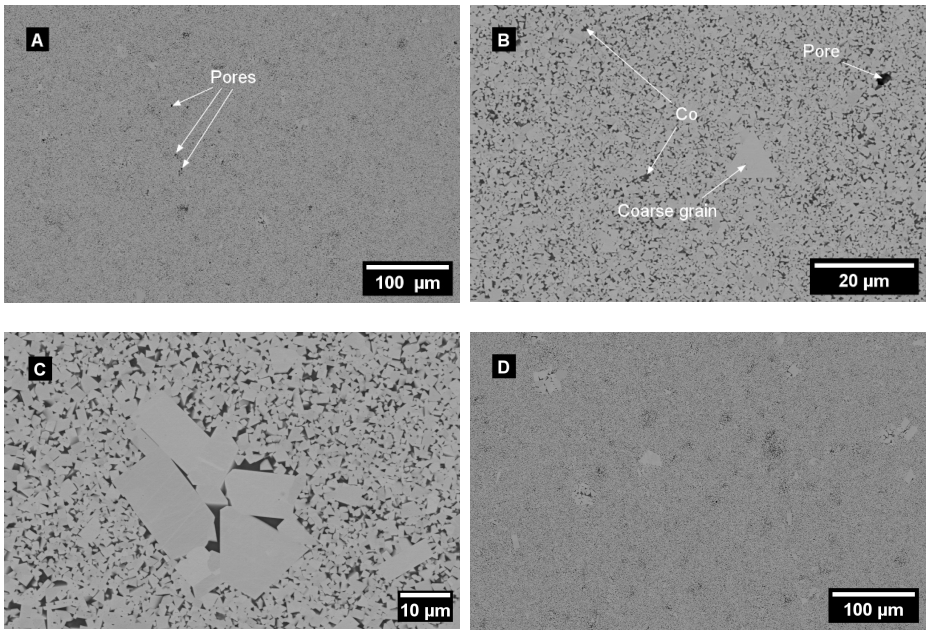

Figure 3. *Cont.*

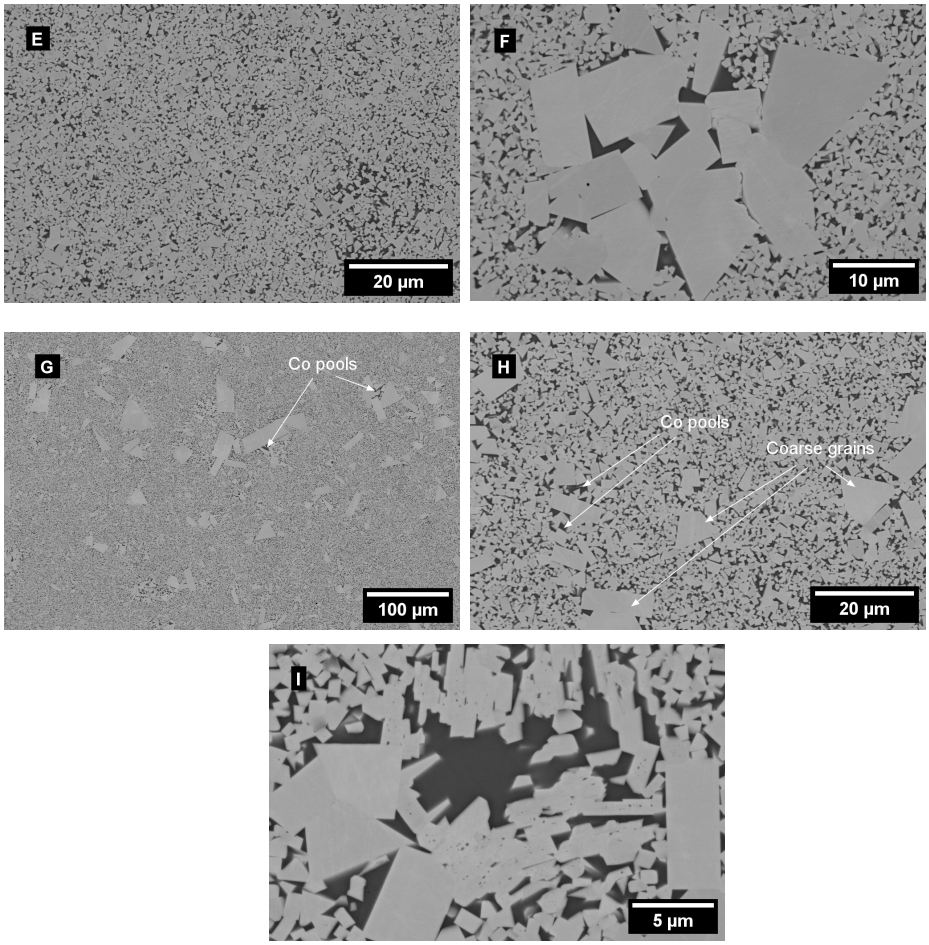

Figure 3. SEM micrographs of the microstructure of 50/60 samples sinter-HIPed at (**A**–**C**) 1400 °C, (**D**–**F**) 1460 °C, and (**G**–**I**) 1500 °C.

Table 2. Grains size, relative density, hardness, and transverse rupture strength of the samples.

Sample	Average Grains Size, µm	Relative Density, %	Area with Grains above 5 µm, %	Hardness, HV_{100}	Transverse Rupture Strength, MPa
1400 50/60	1.65 ± 0.93	98.5 ± 0.6	11	1207 ± 28	1521 ± 149
1460 50/60	1.60 ± 0.92	99.3 ± 0.1	15	1222 ± 16	2295 ± 169
1500 50/60	1.95 ± 1.53	99.8 ± 0.8	32	1140 ± 43	1811 ± 113
1400 50/75	1.61 ± 0.90	98.5 ± 0.5	10	1130 ± 12	2386 ± 300
1460 50/75	1.62 ± 0.92	99.1 ± 0.6	13	1209 ± 47	2600 ± 112
1500 50/75	1.90 ± 1.69	99.5 ± 0.3	24	1167 ± 19	2076 ± 160

With a further increase in temperature up to 1500 °C (micrographs in Figure 3G–I), porosity is further limited: the highest relative density is achieved, as confirmed using the measurements shown in Table 2. Unlike the previous cases, the microstructure in the case of the 1500 °C samples changed drastically. As can be observed in Figure 3H, the grains grow significantly, thus affecting the average grain size, which in this case is 1.95 µm. Additionally, the coarse grain area is more than doubled in comparison to 1460 °C (32% against 15%). The overall average grain size increases together with the difference in size between coarse and fine grains, with some grains showing abnormal growth, reaching almost 90 µm in size. This phenomenon can be explained by the increasing importance of the effects related to coalescence over the densification mechanisms at higher temperatures. The formation of a massive liquid phase combined with high pressure allows for the rapid closure of porosity and promotes the mobility of tungsten and carbon through liquid cobalt,

leading to the growth of larger grains at the expense of smaller ones, according to Ostwald ripening processes, and resulting in a marked bimodality in their size distribution. With the higher magnification (Figure 3I), the stacking of finer grains could be observed, which could be the one of the stages of coalescence of the grains.

The microstructure of the 50/75 samples is presented in Figure 4. The sample after sinter-HIP processing at 1400 °C has some residual porosity, which can be observed at lower and higher magnifications of the SEM image of the transverse section (Figure 4A,B).

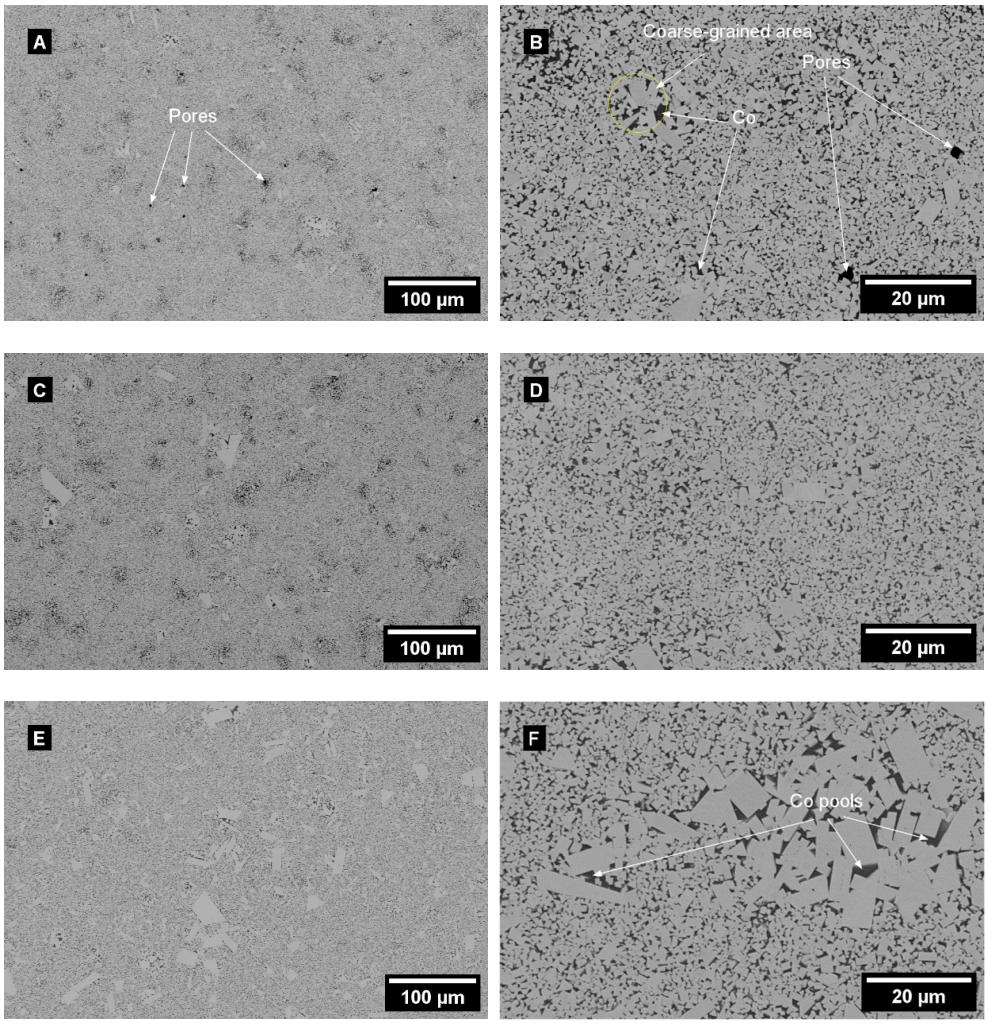

Figure 4. SEM micrographs of the microstructure of 50/75 samples sinter-HIPed at (**A**,**B**) 1400 °C, (**C**,**D**) 1460 °C, and (**E**,**F**) 1500 °C.

The rise in temperature to 1460 °C results in a further densification, and it led to an increase in the area occupied by the coarse WC grains (>5 µm), which could be observed in SEM images in Figure 4C,D and reported in Table 2. The microstructure of the samples sinter-HIPed at 1500 °C shows substantial grain growth both in terms of average grain size and the area occupied by the coarsened WC phase, as shown in Figure 4E,F.

As observed for the samples printed with a binder saturation level of 60%, the relative density progressively increases with the sintering temperature, especially at 1500 °C (Table 2). The formation of cobalt pools in between the coarse-grained areas are similarly promoted during the thermal treatment at higher temperatures. However, both the overall area occupied by the coarsened WC grains and the average grain size remains lower in the parts printed at a binder saturation level of 75%, especially if sinter-HIP processing at 1500 °C is considered.

Binder saturation might affect the amount of residual C, O, and H in the microstructure, since debinding in a non-oxidizing atmosphere should be incomplete. As a result, additional carbon could be introduced into the system, although an estimate of this effect is complex, as both oxygen and hydrogen could lead to decarburization at higher temperatures during the sintering process, thus leading to a counterintuitive reduction of carbon, as observed in previous works [1]. Most likely, the binder saturation level has a minor effect on the densification mechanism, which is dominated by the role of the liquid phase and its amount, the variation of which depends primarily on temperature and secondarily on carbon content. The expected volume of the liquid phase is 25.95% for 1400 °C, 26.62% for 1400 °C, and 27.11% for 1500 °C, as calculated using the CALPHAD method via Thermocalc software (version 2023a, using TCHEA 2 database). Nonetheless, carbon also affects the solubility of tungsten in molten cobalt, the wettability of the surface of the WC grains, and the migration of cobalt toward low carbon regions, as demonstrated in a recent work [2]. The latter mechanism should be irrelevant since binder is initially distributed in the entire component; thus, the compositional gradient is not justified. Instead, the two former factors could influence the growing rate of the WC grains. The grain size characterization in Table 2 suggests that the excess of the binder affects the pore evolution and/or carbon content, leading to a net effect of grain growth inhibition. The difference between printing conditions becomes particularly evident at a higher sinter-HIP temperature (1500 °C), because it favors diffusivity in the liquid phase when not inhibited, as was observed.

The negligible effect of binder saturation on the phase composition was verified using an XRD analysis (Figure 5) as well. Diffractograms showed no relevant differences among the 50/60 and 50/75 samples. In addition, meaningful variations induced with sintering temperatures were not detected. Indeed, peaks of WC and low intensity peaks of Co are observed. No carbon or secondary phases, such as undesired low carbon carbides, were identified. This suggests that the minor W_2C phases in the feedstock are properly carburized during the densification process, likely thanks to the carbon introduced with the organic binder during the shaping phase. The elemental map of the distribution of the chemical elements (Figure 5B) showed the distribution of cobalt in between the WC grains.

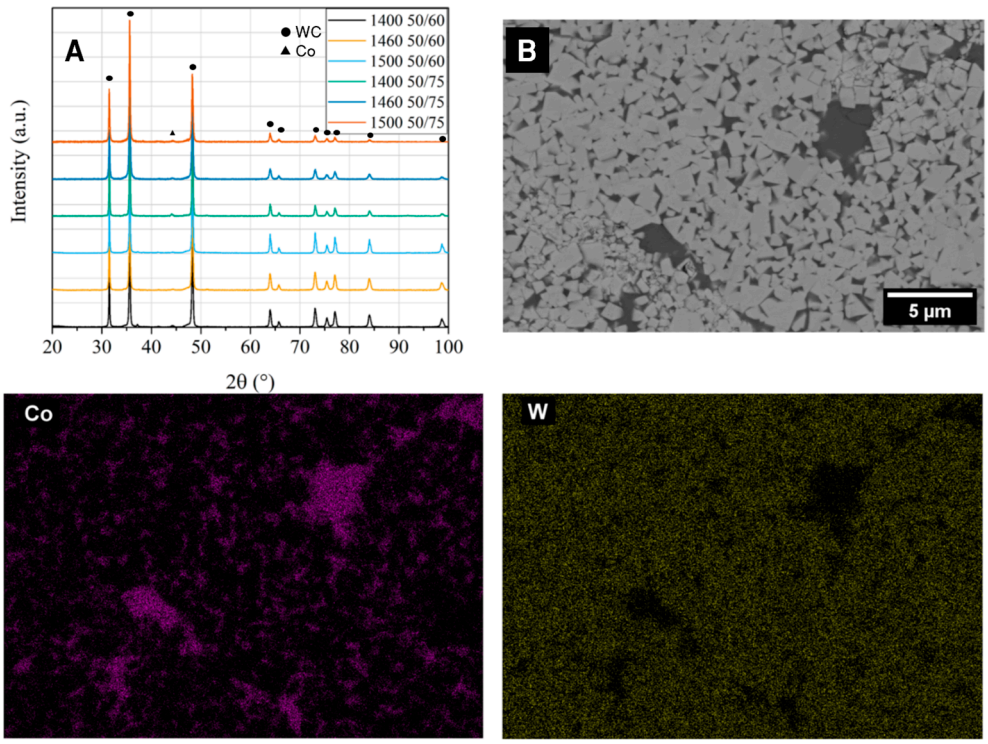

Figure 5. (**A**) XRD patterns of WC–12Co 50/60 and 50/70 sinter-HIPed samples at all sintering temperatures; (**B**) Elemental mapping of sinter-HIPed sample.

3.3. Mechanical Characterization

The transverse rupture strength (TRS) was determined using a three-point bending test, which was described in Section 2. There is a positive trend of the TRS (Figure 6A) with increasing temperatures of sinter-HIP processing from 1400 °C to 1460 °C, which, in accordance with observations on the microstructure, is justified by the reduction of the overall porosity without a significant growth of the average grain size. The further increase to 1500 °C causes an opposite effect. In this case, the reduction of the TRS is associated with the growth of the WC grains and the formation of large cobalt pools among them, which has already been described (Figures 3 and 4). Moreover, the increase in the binder saturation level during the printing of the samples from 60% to 75% leads to an increase in the TRS in the whole range of the sinter-HIP temperatures investigated, due to the concomitant achievement of matching final densities and the reduced average grain size. The highest increase in the TRS is noticed at the lowest temperature (1400 °C). In addition, the green parts of the samples with a higher BS better retained geometric shapes during handling. With an increase in the sinter-HIP temperature, the influence of the increased binder saturation level on the TRS becomes less relevant. Hardness shows a similar behavior in correspondence with sinter-HIP temperature: it increases from 1400 °C to 1460 °C, and then decreases at 1500 °C.

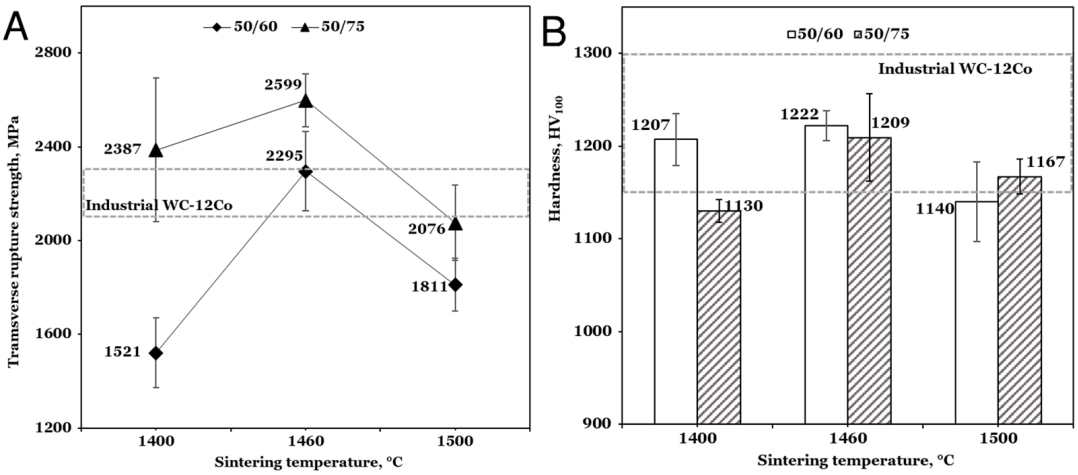

Figure 6. (**A**) results of three-point bending tests; (**B**) results of hardness measurements, data about industrial WC–12Co from [27].

When considering the fracture behaviour of the samples at 1400 °C, it was observed that porosity is the dominant cause of the sample failure, whereas at 1460 °C and 1500 °C, the main cause shifts toward coarse WC grains, where cracks initiate and lead to sample failure. The sample failure is similar for both binder saturation levels, and it does not change with an increase in the binder saturation level to 75% (as shown in Figure 7).

In comparison to the transverse rupture strength of the samples produced using traditional technologies, the result of the samples sinter-HIPed at 1460 °C lies within or above the typical values of WC–12Co, especially for the samples printed with a 75% binder saturation level. The latter shows less scattered results, which can indicate that this printing setup provided more predictable and repeatable properties. Satisfactory results were also obtained for samples sinter-HIPed at 1400 °C; however, the scattering is significant: this is due to the higher porosity, which may anticipate the failure of the component. Samples with an excessive grain growth (sinter-HIPed at 1500 °C) are generally weaker than other samples.

Regarding the microhardness, the trend is similar. For samples sinter-HIPed at 1460 °C, the Vickers hardness (Figure 6B) lies within the typical values for traditionally manufactured cemented carbides at both 60% and 75% binder saturation levels. At

1400 °C and 1500 °C, the performance is slightly inferior, and eventually it does not satisfy industrial requirements.

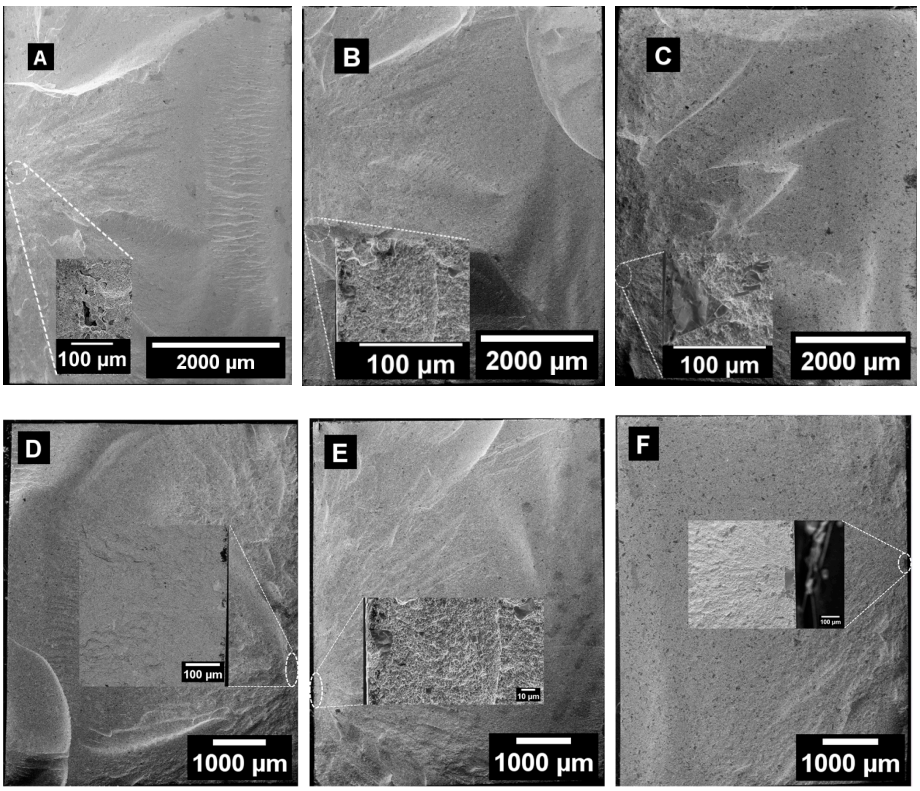

Figure 7. SEM image of fractured samples sinter-HIPed at (**A**) 1400 °C, (**B**) 1460 °C, (**C**) 1500 °C (binder saturation of 60%), (**D**) 1400 °C, (**E**) 1460 °C, and (**F**) 1500 °C (binder saturation of 75%).

3.4. Defects

Some specific defects could be observed during the binder-jetting process which are worthy of being discussed. Firstly, some discarded samples featured localized porosity due to discontinuities in the printing process, namely printing interruption due to the need to refill the powder hopper. This leads to a discontinuity in the delivery process of the organic binder and in its infiltration mechanisms, thus leading to heterogeneous porosity within the components (Figure 8A).

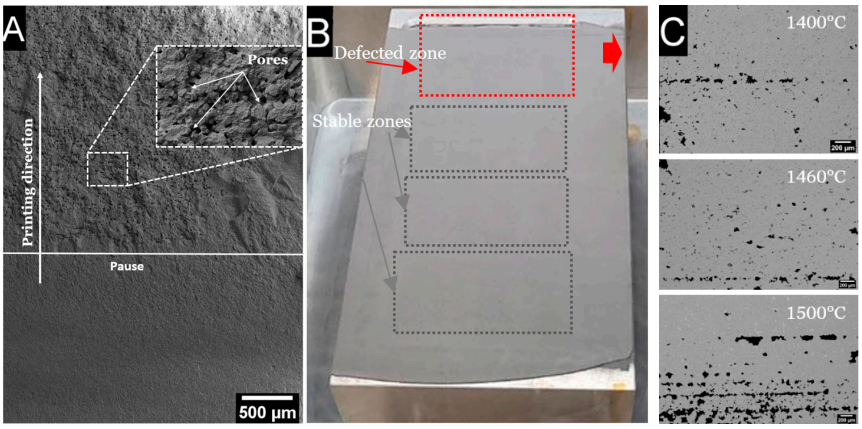

Figure 8. (**A**) SEM images of defects caused by printing interruption on a fracture surface; (**B**) general view of the powder bed with defected zone; (**C**) microstructure of defected sectioned samples.

Another cause of the defects is related to the non-uniform distribution of feedstock on the powder bed, possibly due to insufficient filling close to the job plate boundaries or to friction among the powder bed volume and the external fixed walls during the vertical downshifting of the printing platform. In this case, some of the corner regions of the parts might have incomplete powder particle packing (especially close to the border of the building platform) (Figure 8B). This could cause the appearance of porosity of a relevant size, which cannot be eliminated or sufficiently reduced with an increase in the sintering temperature (Figure 8C).

The abovementioned binder-jetting-related defects should be taken into consideration during the technological manufacturing process, to avoid possible risks of failure and ensure good repeatability of the results with predictable and stable microstructures and properties comparable to industrial-scale traditional technologies. In this study, the investigation was performed on samples taken from the central zone of the powder bed to ensure the stability and repeatability of the results.

4. Conclusions

In the current study, the influence of sinter-HIP temperature and binder saturation level on the microstructure and the mechanical properties of binder-jetted additively manufactured WC–12Co was investigated.

The microstructure of the samples after sinter-HIP processing at 1400 °C consists of two zones: mainly a fine-grained microstructure and localized regions of coarse grains of WC surrounded by cobalt pools. With the increase in the temperature of sinter-HIP processing from 1400 °C to 1460 °C, the residual pores were mostly filled, with a slight increase in coarse-grained areas. A further raise in temperature to 1500 °C leads to a significant coalescence of the WC phase, leading to abnormal grain growth. The increase in binder-jetting saturation level from 60% to 75% leads to a slight decrease in the density for the samples. The increase in binder saturation during printing leads to the better repeatability of the printing procedure and to the safer handling of the components due to the higher sturdiness of the green parts.

The transverse rupture strength and hardness increase with the sinter-HIP temperature from 1400 °C to 1460 °C, and then decrease for the samples treated at 1500 °C. This trend could be explained by the complete filling of the pores in the first segment and by the prevailing significant growth of WC grains in the second one.

During the usage of binder jetting, some specific potential defects should be taken into consideration, such as the risk of the formation of increased porosity in between the layers due to process interruptions and insufficient powder filling at the sides of the job plate, leading to relevant localized porosity that cannot be reduced or eliminated, regardless of the sinter-HIP temperature.

Author Contributions: Conceptualization, I.G., A.P., N.L. and M.V.; methodology, N.L. and M.V.; investigation, I.G., M.M. and G.P.D.G.; resources, G.P.D.G.; writing—original draft, I.G.; writing—review & editing, G.P.D.G., N.L. and M.V.; supervision, A.P., N.L. and M.V. All authors have read and agreed to the published version of the manuscript.

Funding: This research received no external funding.

Data Availability Statement: The raw data supporting the conclusions of this article will be made available by the authors on request.

Acknowledgments: The authors would like to acknowledge the "Functional Sintered Materials (Funtasma)" Interdepartmental Laboratory of Politecnico di Milano. The authors would like to acknowledge the support given by Sandra Tedeschi for the preparation and analysis of the sinter-HIP samples at HI.Lab.

Conflicts of Interest: Author Gian Pietro De Gaudenzi was employed by the company F.I.L.M.S. S.p.A., OMCD Group. The remaining authors declare that the research was conducted in the absence of any commercial or financial relationships that could be construed as a potential conflict of interest.

References

1. Ettmayer, P.; Kolaska, H.; Ortner, H.M. History of Hardmetals. In *Comprehensive Hard Materials*; Sarin, V., Mari, D., Llanes, L., Eds.; Elsevier: Amsterdam, The Netherlands, 2014; pp. 3–27.
2. Marshall, J.M.; Kusoffsky, A. Binder phase structure in fine and coarse WC–Co hard metals with Cr and V carbide additions. *Int. J. Refract. Met. Hard Mater.* **2013**, *40*, 27–35. [CrossRef]
3. García, J.; Ciprés, V.C.; Blomqvist, A.; Kaplan, B. Cemented carbide microstructures: A review. *Int. J. Refract. Met. Hard Mater.* **2019**, *80*, 40–68. [CrossRef]
4. Gee, M.; Gant, A.; Roebuck, B. Wear mechanisms in abrasion and erosion of WC/Co and related hardmetals. *Wear* **2007**, *263*, 137–148. [CrossRef]
5. Padmakumar, M. Additive Manufacturing of Tungsten Carbide Hardmetal Parts by Selective Laser Melting (SLM), Selective Laser Sintering (SLS) and Binder Jet 3D Printing (BJ3DP) Techniques. *Lasers Manuf. Mater. Process.* **2020**, *7*, 338–371. [CrossRef]
6. Uhlmann, E.; Bergmann, A.; Gridin, W. Investigation on Additive Manufacturing of Tungsten Carbide-cobalt by Selective Laser Melting. *Procedia CIRP* **2015**, *35*, 8–15. [CrossRef]
7. Grigoriev, S.; Tarasova, T.; Gusarov, A.; Khmyrov, R.; Egorov, S. Possibilities of Manufacturing Products from Cermet Compositions Using Nanoscale Powders by Additive Manufacturing Methods. *Materials* **2019**, *12*, 3425. [CrossRef] [PubMed]
8. Chen, J.; Huang, M.; Fang, Z.Z.; Koopman, M.; Liu, W.; Deng, X.; Zhao, Z.; Chen, S.; Wu, S.; Liu, J.; et al. Microstructure analysis of high density WC-Co composite prepared by one step selective laser melting. *Int. J. Refract. Met. Hard Mater.* **2019**, *84*, 4980. [CrossRef]
9. Ku, N.; Pittari, J.J.; Kilczewski, S.; Kudzal, A. Additive Manufacturing of Cemented Tungsten Carbide with a Cobalt-Free Alloy Binder by Selective Laser Melting for High-Hardness Applications. *JOM* **2019**, *71*, 1535–1542. [CrossRef]
10. Xiong, Y.; Smugeresky, J.E.; Ajdelsztajn, L.; Schoenung, J.M. Fabrication of WC–Co cermets by laser engineered net shaping. *Mater. Sci. Eng. A* **2008**, *493*, 261–266. [CrossRef]
11. Davoren, B.; Sacks, N.; Theron, M. Laser engineered net shaping of WC-9.2wt%Ni alloys: A feasibility study. *Int. J. Refract. Met. Hard Mater.* **2019**, *86*, 105136. [CrossRef]
12. Lengauer, W.; Duretek, I.; Fürst, M.; Schwarz, V.; Gonzalez-Gutierrez, J.; Schuschnigg, S.; Kukla, C.; Kitzmantel, M.; Neubauer, E.; Lieberwirth, C.; et al. Fabrication and properties of extrusion-based 3D-printed hardmetal and cermet components. *Int. J. Refract. Met. Hard Mater.* **2019**, *82*, 141–149. [CrossRef]
13. Kitzmantel, M.; Lengauer, W.; Duretek, I.; Schwarz, V.; Kukla, C.; Lieberwirth, C.; Morrison, V.; Wilfinger, T.; Neubauer, E. Potential of Extrusion Based 3D-printed Hardmetal and Cermet Parts. In Proceedings of the World PM 2018, Bilbao, Spain, 14–18 October 2018; pp. 938–945.
14. Jucan, O.-D.; Gădălean, R.-V.; Chicinaș, H.-F.; Bâlc, N.; Popa, C.-O. The Assessment of the Transversal Rupture Strength (TRS) and Hardness of WC-Co Specimens Made via Additive Manufacturing and Sinter-HIP. *Metals* **2023**, *13*, 1051. [CrossRef]
15. Cramer, C.L.; Aguirre, T.G.; Wieber, N.R.; Lowden, R.A.; Trofimov, A.A.; Wang, H.; Yan, J.; Paranthaman, M.P.; Elliott, A.M. Binder jet printed WC infiltrated with pre-made melt of WC and Co. *Int. J. Refract. Met. Hard Mater.* **2020**, *87*, 5137. [CrossRef]
16. Mudanyi, R.K.; Cramer, C.L.; Elliott, A.M.; Unocic, K.A.; Guo, Q.; Kumar, D. W-ZrC composites prepared by reactive melt infiltration of Zr2Cu alloy into binder jet 3D printed WC preforms. *Int. J. Refract. Met. Hard Mater.* **2020**, *94*, 105411. [CrossRef]
17. Arnold, J.M.; Cramer, C.L.; Elliott, A.M.; Nandwana, P.; Babu, S.S. Microstructure evolution during near-net-shape fabrication of NixAly-TiC cermets through binder jet additive manufacturing and pressureless melt infiltration. *Int. J. Refract. Met. Hard Mater.* **2019**, *84*, 104985. [CrossRef]
18. Cabezas, L.; Berger, C.; Jiménez-Piqué, E.; Pötschke, J.; Llanes, L. Testing length-scale considerations in mechanical characterization of WC-Co hardmetal produced via binder jetting 3D printing. *Int. J. Refract. Met. Hard Mater.* **2023**, *111*, 6099. [CrossRef]
19. Enneti, R.K.; Prough, K.C. Effect of binder saturation and powder layer thickness on the green strength of the binder jet 3D printing (BJ3DP) WC-12%Co powders. *Int. J. Refract. Met. Hard Mater.* **2019**, *84*, 4991. [CrossRef]
20. Enneti, R.K.; Prough, K.C. Wear properties of sintered WC-12%Co processed via Binder Jet 3D Printing (BJ3DP). *Int. J. Refract. Met. Hard Mater.* **2018**, *78*, 228–232. [CrossRef]
21. Wolfe, T.; Shah, R.; Prough, K.; Trasorras, J.L. Coarse cemented carbide produced via binder jetting 3D printing. *Int. J. Refract. Met. Hard Mater.* **2023**, *110*, 6016. [CrossRef]
22. Wolfe, T.; Shah, R.; Prough, K.; Trasorras, J. Binder jetting 3D printed cemented carbide: Mechanical and wear properties of medium and coarse grades. *Int. J. Refract. Met. Hard Mater.* **2023**, *113*, 6197. [CrossRef]
23. Mariani, M.; Goncharov, I.; Mariani, D.; De Gaudenzi, G.P.; Popovich, A.; Lecis, N.; Vedani, M. Mechanical and microstructural characterization of WC-Co consolidated by binder jetting additive manufacturing. *Int. J. Refract. Met. Hard Mater.* **2021**, *100*, 5639. [CrossRef]
24. Mariani, M.; Mariani, D.; De Gaudenzi, G.P.; Lecis, N. Effect of printing parameters on sintered WC-Co components by binder jetting. *Eur. J. Mater.* **2022**, *2*, 365–380. [CrossRef]
25. Schneider, C.A.; Rasband, W.S.; Eliceiri, K.W. NIH Image to ImageJ: 25 Years of image analysis. *Nat. Methods* **2012**, *9*, 671–675. [CrossRef] [PubMed]
26. *ASTM B311-17*; Standard Test Method for Density of Powder Metallurgy (PM) Materials Containing Less Than Two Percent Porosity. ASTM: West Conshohocken, PA, USA, 2017.

27. *ASTM C1327*; Vickers Indentation Hardness of Ceramics. ASTM: West Conshohocken, PA, USA, 2015.
28. *ISO 3327:2009*; Hardmetals. Determination of Transverse Rupture Strength. ISO: Geneva, Switzerland, 2009.